Functional Activity of Photoreceptor Cyclic Nucleotide-Gated Channels Is Dependent on the Integrity of Cholesterol- and Sphingolipid-Enriched Membrane Domains†

Xi-Qin Ding,*,‡ J. Browning Fitzgerald,‡ Alexander V. Matveev,‡ Mark E. McClellan,§ and Michael H. Elliott§

Departments of Cell Biology and Ophthalmology, University of Oklahoma Health Sciences Center, Dean A. McGee Eye Institute, Oklahoma City, Oklahoma 73104

Received September 30, 2007; Revised Manuscript Received January 15, 2008

ABSTRACT: Rod and cone photoreceptor cyclic nucleotide-gated (CNG) channels play pivotal roles in phototransduction. This work investigates the functional significance of photoreceptor CNG channel association with membrane microdomains enriched in raft lipids, cholesterol and sphingolipids. The primary subunits of cone and rod CNG channels, CNGA3 and CNGA1, respectively, were heterologously expressed in HEK 293 cells, and channel activity was determined by ratiometric measurement of $[Ca^{2+}]_i$ in response to cyclic guanosine monophosphate (cGMP) stimulation. CNGA3 was found to be largely insoluble following Triton X-100 extraction and cofractionationed with biochemically isolated membrane domains enriched in caveolin-1. Cofractionation of both natively expressed CNGA3 and CNGB1 (the modulatory subunit of the rod CNG channel) with the low buoyant density, caveolin-1-enriched membranes was also confirmed in mouse retinas. The functional significance of this association was established by the observed negative effects of depletion of raft lipids on the channel activity. Treatment with the cholesterol depleting agent, methyl-β-cyclodextrin (MCD), significantly inhibited CNGA3 and CNGA1 activation in response to cGMP stimulation. MCD treatment lowered cellular cholesterol levels by ~45% without altering fatty acid composition, suggesting that the inhibition of channel activity by MCD treatment is not due to perturbation of other membrane lipids. Treatment with the sphingolipid biosynthesis inhibitor myriocin resulted in impaired activation and cytosolic redistribution of CNGA3, suggesting that the integrity of the membrane domains is critical for the channel cellular processing and plasma membrane localization. This study demonstrates the association of photoreceptor CNG channels with membrane domains enriched in raft lipids and indicates, for the first time, that raft lipids modulate the plasma membrane localization and functional activity of photoreceptor CNG channels.

Rod and cone photoreceptor cyclic nucleotide-gated (CNG)[1] channels are essential for phototransduction. They control the flow of cations into the outer segment (OS) in response to light-mediated changes in intracellular cyclic guanosine monophosphate (cGMP) concentration (*1*). Photoreceptor CNG channels are localized to the plasma membranes of both rod and cone OSs (*2, 3*). In the dark, rod channels are activated by the binding of cGMP, allowing a steady cation current. Light triggers a sequence of enzymatic reactions that leads to the hydrolysis of cGMP resulting in CNG channel closure, reduction in inward current, and membrane hyperpolarization (*4*). A similar transduction scheme exists in cones, which are responsible for vision in bright light and color vision. Mutations in the rod CNG channel are associated with retinitis pigmentosa while mutations in the cone CNG channel are highly linked to various forms of achromatopsia and cone-rod dystrophy (*5, 6*). Indeed, about 70 mutations have been identified to date in genes encoding cone CNG channel subunits (*7–9*), accounting for nearly 70% of patients with achromatopsia and early onset macular degeneration (onset under age 50) (*7*).

Native photoreceptor CNG channels are heteromeric complexes composed of two structurally related subunit types, CNGA1 and CNGB1 for the rod channel and CNGA3 and CNGB3 for the cone channel. To function as a membrane signaling complex, the CNG channel requires proper intersubunit interactions and associations with adjacent proteins. Targeting of photoreceptor CNG channels to specific regions of the plasma membrane rich in phototransduction molecules is critical for efficient and

† This work was supported by grants from the National Center for Research Resources (P20RR017703), the National Eye Institute (P30EY12190), the American Health Assistance Foundation (Macular Degeneration Research Grant Award), and The Foundation Fighting Blindness and an unrestricted grant from Research to Prevent Blindness, Inc., to the Department of Ophthalmology at the University of Oklahoma Health Sciences Center.

* Address correspondence to this author. Phone: 405-271-8001ext 47966. Fax: 405-271-3548. E-mail: xi-qin-ding@ouhsc.edu.

‡ Department of Cell Biology, University of Oklahoma Health Sciences Center.

§ Department of Ophthalmology, University of Oklahoma Health Sciences Center.

[1] Abbreviations: CNG, cyclic nucleotide-gated; cGMP, cyclic guanosine monophosphate; OS, outer segment; DRMs, detergent-resistant membranes; TfR, transferrin receptor; GARP, glutamic acid-rich protein; MCD, methyl-β-cyclodextrin; KI, potassium iodide; OG, octyl glucoside; HEK, human embryonic kidney; DMEM, Dulbecco's modified Eagle's medium; PBS, phosphate-buffered saline.

10.1021/bi7019645 CCC: $40.75
Published on Web 02/28/2008

spatially confined responses to stimuli. In fact, a number of disease-causing mutations in rod and cone photoreceptor CNG channels are associated with impaired plasma membrane localization and cytosolic accumulation of the channel (*10, 11*).

Although there is increasing information about CNG channel structure and function, our understanding of the relevance of the membrane environment on channel activity is quite limited. Recently, evidence has accumulated showing the participation of protein–lipid interactions in protein membrane targeting, localization, and function (*12–14*). There is recent evidence showing that some important functional interactions between channels and lipids take place in specialized microdomains ("lipid rafts") within the plane of the plasma membrane (*15–17*). These domains are characterized by tightly packed cholesterol and sphingolipids, resistance to nonionic detergent solubilization, and low buoyant density (*18, 19*). Some membrane proteins including signal transduction enzymes, membrane receptors, and ion channels are enriched in lipid rafts (*16, 17, 20–22*). For instance, isoform-specific localization of voltage-gated K^+ channels to distinct lipid raft populations has been described by Martens et al. (*17, 23*), and association of the olfactory CNG channel with lipid rafts and the role of raft lipids on this channel's activation have been demonstrated by Brady et al. (*15*). Indeed, disruption of lipid rafts by depleting cholesterol or inhibition of sphingolipid biosynthesis has been shown to disorder a number of signaling events such as β-adrenergic signaling (*24*), T-cell activation (*25*), and ion channel function (*15, 16, 26*). Lipid rafts have also been proposed to be involved in the sorting of proteins in the Golgi and their delivery to the plasma membrane (*19*).

The role of lipid rafts in photoreceptor CNG channel activity is unidentified. However, a recent proteomic analysis identified the rod CNG channel as an abundant component of detergent-resistant membranes (DRMs) derived from rod OS membranes (*27*). Hampered cellular processing and membrane localization of photoreceptor CNG channels represent a common mechanism of channel dysfunction (*10, 11, 28*), and the significance of lipid domains in these processes is important to understand. On this basis, the present study was designed to examine the association of photoreceptor CNG channels with raft lipids in both the heterologous expression system and retina. We used wild-type mouse retina (rod-dominant) to study the native rod CNG channel and retinas of mice deficient in the transcription factor neural retina leucine zipper (Nrl) (cone-dominant) (*29*) for the native cone CNG channel study. The protein Nrl is a basic-motif leucine zipper transcription factor that is preferentially expressed in rod photoreceptors and is essential for the normal development of rods. Mice lacking the *Nrl* gene have no rods but have increased numbers of S-cones, manifested as the loss of rod function and supernormal cone function (*29*). Here, we report that both cone and rod CNG channels associate with membrane domains and that the lipid environment of these domains modulates channel function and membrane localization.

EXPERIMENTAL PROCEDURES

Materials and Animals. Mouse CNGA3 cDNA was amplified from a mouse retinal cDNA library using the forward primer 5′-CGCGGATCCGCGTGAATGTGACCT-GTGCAGAGATGG-3′ and the reverse primer 5′-CCGCTC-GAGCGGGGCAGAGCCACCTGCATTTTCAGTCAG-3′ and ligated into the *Bam*HI and *Xho*I sites of pcDNA3.1 (Invitrogen, Carlsbad, CA). Green fluorescent protein- (GFP-) CNGA3 was constructed through conventional cloning procedures using the fusion protein vector pEGFP-C1 from Clontech. DNA sequencing was carried out to confirm the composition of all constructs. Mouse CNGB3 cDNA was kindly provided by Dr. Martin Biel (Ludwig-Maximilians-Universität München, München, Germany), and human CNGA1 cDNA was kindly provided by Dr. William Zagotta (University of Washington, Seattle, WA). Human transferrin receptor (hTfR) cDNA was generously provided by Dr. Michael Marks (University of Pennsylvania School of Medicine). Rabbit polyclonal antibody against a peptide corresponding to the sequence between residues 77 and 97 (SNAQPNPGEQKPPDGGEGRKE) of the mouse CNGA3 was generated and used for Western blotting. The rat monoclonal antimouse CNGA3 antibody was kindly provided by Dr. Benjamin Kaupp (Institut für Biologische Informationsverarbeitung, Forschungszentrum, Jülich, Germany) and used for immunolabeling. The monoclonal antibody against the glutamic acid-rich protein (GARP) was generously provided by Dr. Robert Molday (University of British Columbia, Vancouver, Canada). Polyclonal antibody against caveolin-1 was purchased from BD Biosciences (Lexington, KY); monoclonal anti-actin antibody was purchased form Abcam, Inc. (Cambridge, MA); and the monoclonal anti-TfR antibody was purchased from ZYMED Laboratories (Carlsbad, CA). Methyl-β-cyclodextrin (MCD), cholesterol, 8-pCPT-cGMP, and potassium iodide (KI) were from Sigma-Aldrich (St. Louis, MO). Myriocin (SPI-1) was purchased from BIOMOL International, L.P. (Plymouth Meeting, PA). Lipid standards were purchased from Nu-Chek Prep (Elysian, MN) or Sigma-Aldrich. All other chemicals were purchased from Fisher Scientific (Pittsburgh, PA), Sigma-Aldrich (St. Louis, MO), or Invitrogen (Carlsbad, CA).

Wild-type mice (C57BL background) were purchased from Charles River Laboratories, Inc. (Wilmington, MA), and $Nrl^{-/-}$ mice were kindly provided by Dr. Anand Swaroop (University of Michigan, Ann Arbor, MI). Retinas from these mice were used for membrane preparation and isolation of detergent-resistant membranes. All experiments and animal maintenance were approved by the local Institutional Animal Care and Use Committee (Oklahoma City, OK) and conformed to the guidelines on the care and use of animals adopted by the Society for Neuroscience and the Association for Research in Vision and Ophthalmology (Rockville, MD).

Cell Culture and Transfection. Human embryonic kidney (HEK) 293 cells were routinely cultured in Dulbecco's modified Eagle's medium (DMEM) supplemented with 10% fetal bovine serum and 1% penicillin/streptomycin at 37 °C in a humidified atmosphere with 5% CO_2. Cells were transfected at 70−80% confluence with mouse CNGA3 or hTfR cDNAs (20 μg per 100 mm dish) by the calcium phosphate method and used for experiments ~48 h post-transfection.

Cell Membrane Preparation and Detergent Solubilization. To assess detergent solubility, total cellular and retinal membranes were prepared. Cells or retinas were homog-

enized in homogenization buffer (10 mM Tris-HCl, pH 7.4, 1 mM EDTA, 200 mM sucrose, 1 mM phenylmethanesulfonyl fluoride). The nuclei and cell debris were removed from the homogenate by centrifugation at 900*g* for 10 min at 4 °C. The resulting supernatant was centrifuged at 16000*g* for 30 min at 4 °C. The membrane pellet was solubilized in homogenization buffer containing 1% Triton X-100 or 60 mM octyl glucoside (OG) for 4 h at 4 °C. The detergent: membrane protein ratios for Triton X-100 and OG solubilizations were 3.3:1 and 5:1 (M/M), respectively. For HEK 293 cells, the average detergent:phospholipid molar ratio was determined to be 6:1. Given that we recover ~90 nmol of phospholipid/retina (no significant difference between wild-type and $Nrl^{-/-}$ retina), the detergent:phospholipid molar ratio can be estimated as 3.6–5:1 and 13:1 for the solubilization by Triton X-100 (0.5–1.0%) and OG (60 mM), respectively. After removal of supernatants, the pellets were resuspended in phosphate-buffered saline (PBS), and both pellets and supernatants were mixed with Laemmli sample buffer for electrophoresis and immunoblotting.

Isolation of Triton X-100-Resistant, Low Buoyant Density Membrane Domains. Isolation of low-density, Triton X-100-insoluble complexes was performed essentially as described previously (*30, 31*). Briefly, cells or retinal membrane preparations were homogenized in buffer A [10 mM Tris-HCl (pH 7.4), 70 mM NaCl, 2 mM $MgCl_2$, 0.1 mM EGTA] followed by solubilization with ice-cold 1% Triton X-100 (detergent:phospholipid ratios = 6:1 for cell and 5:1 for retinal membranes). The sucrose content was raised to 0.9 M by addition of 2.4 M sucrose in buffer A, and the solubilized homogenates were layered at the bottom of discontinuous sucrose gradients [0.8, 0.7, 0.6, and 0.5 M sucrose in buffer B containing 10 mM Tris-HCl (pH 7.4), 70 mM NaCl, 2 mM $MgCl_2$, and 0.5 mM EDTA]. The gradients were centrifuged at 250000*g* for 20 h at 4 °C, and 0.5 mL fractions were collected from the top of the gradients and subjected to 10% SDS−PAGE and Western blot analysis.

Depletion and Repletion of Cellular Cholesterol and Inhibition of Sphingolipid Biosynthesis. Cellular cholesterol depletion was achieved by incubating cells in 2% MCD in serum-free media at 37 °C for 1 h. For cholesterol repletion experiments, cells were treated with 2% MCD in the presence of cholesterol (0.5 mM, Sigma) at 37 °C for 1 h followed by calcium assays. To inhibit biosynthesis of sphingolipids, cells in DMEM medium were treated with SPI-1 at concentrations of 0.3, 1.0, and 5.0 μM at 37 °C for 72 h prior to use in the experiments.

Lipid Analysis. Analyses of cholesterol and fatty acids were performed essentially as described previously (*31*) using a two-part extraction procedure to separate saponifiable from nonsaponifiable lipids. Briefly, samples were supplemented with internal standards [19-hydroxycholesterol (Steraloids, Inc., Newport, RI) and 15:0, 17:0, and 21:0 fatty acid standards (Nu-Chek Prep, Elysian, MN)] prior to saponification with 2% (w/v) KOH in ethanol at 100 °C for 1 h. Distilled H_2O (3 mL) was added, the nonsaponifiable lipids were extracted three times into hexane, and the recovered organic phases were pooled. The aqueous phase was acidified by addition of 200 μL of concentrated HCl and sonicated for 10 min prior to extraction three times into hexane (this organic phase contains saponified fatty acids). Both saponifiable and nonsaponifiable lipid extracts were dried under N_2, and the nonsaponifiable lipids were resuspended in 50 μL of methanol for HPLC injection. Cholesterol was separated on a C18 column (Supelcosil LC-18, 25 cm × 4.6 mm, 5 μm particle size) with an isocratic mobile phase of 1 mL/min methanol. Detection was at 208 nm using an Agilent 1100 series photodiode array detector; cholesterol was quantified based upon absorbance at 208 nm, in comparison with an authentic cholesterol standard (within the linear response range), and corrected for recovery of the 19-hydroxycholesterol internal standard. The fatty acid extract was analyzed as described previously (*30*).

SDS−PAGE and Western Blot. The Triton X-100-solubilized membrane proteins were assayed for protein concentration using a Bio-Rad protein assay kit (Bio-Rad Laboratories, Hercules, CA). For Western blotting, the protein samples were subjected to 10% SDS−PAGE and transferred to polyvinylidene difluoride (PVDF) membranes. Blots were incubated with the appropriate primary antibody at a dilution ratio of 1:250 (anti-CNGA3), 1:250 (anti-caveolin-1), 1:5000 (anti-actin), 1:250 (anti-TfR), or 1:50 (anti-GARP) for 2 h at room temperature. After three 10 min washings with 1× TBST (Tris-buffered saline with Tween 20), the blots were incubated with horseradish peroxidase-conjugated anti-rabbit or anti-mouse secondary antibody (1:12500) for 1 h at room temperature. After being rinsed several times with 1× TBST, SuperSignal chemiluminescent substrate (Pierce, Rockford, IL) was applied to detect binding of the primary antibodies to their cognate antigens.

Assessment of the Channel Activity by Ratiometric Measurement of $[Ca^{2+}]_i$. The fluorescent indicator Indo-1/AM was used to monitor Ca^{2+} influx through CNGA3 channels in cell suspensions. The assays were performed as described by Ma et al. (*32*) using a PTI QuantaMaster spectrofluorometer (Photon Technology International). This assay is designed to determine CNG channel activity in cell populations (2×10^6) in response to cGMP stimulation. Briefly, cells (36–48 h posttransfection) were harvested with cell dissociation medium (Invitrogen), washed with the extracellular solution (ECS; 140 mM NaCl, 5 mM KCl, 1 mM $MgCl_2$, 1.8 mM $CaCl_2$, 10 mM glucose, 15 mM HEPES, pH 7.4), and loaded with 2 μM Indo-1/AM (Sigma-Aldrich) in ECS in the presence of 0.05% Pluronic F-127 (Invitrogen) for 40 min at room temperature. After the 40 min incubation, cells were washed three times with ECS and resuspended in ECS (1×10^6/mL). Ca^{2+} entry in response to 8-pCPT-cGMP was determined by ratiometric measurement which represents free intracellular Ca^{2+} concentrations. Changes of intracellular Ca^{2+} concentration were expressed as a Δ340/380 ratio. Data were analyzed and graphed using GraphPad Prism software (GraphPad Software, San Diego, CA).

Immunofluorescence Labeling and Confocal Microscopy. Immunofluorescence labelings were performed as described previously (*33*). HEK 293 cells were grown in DMEM on coverslips precoated with fibronectin (Sigma-Aldrich). Cells were washed for 3 × 5 min with PBS, fixed with 4% (w/v) paraformaldehyde for 10 min at room temperature, washed again for 3 × 5 min with PBS, permeabilized with 0.3% (v/v) Tween 20 (Bio-Rad Laboratories) in PBS for 15 min at room temperature, and then blocked for 1 h at room temperature in 5% BSA in PBS. The rat monoclonal anti-

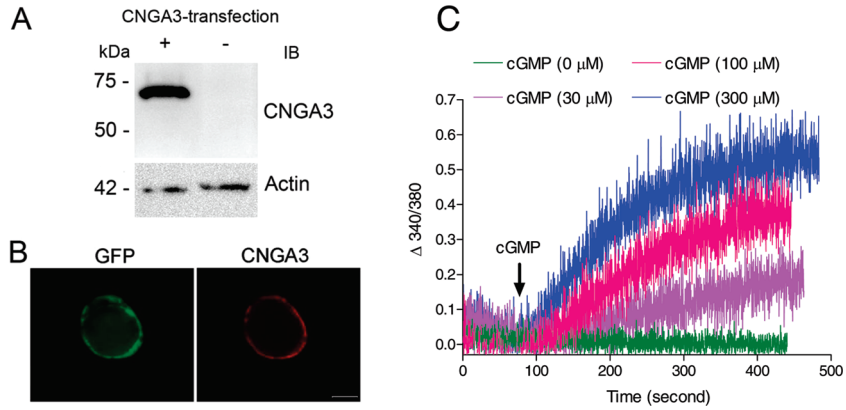

FIGURE 1: Functional expression of mouse CNGA3 in HEK 293 cells. (A) Western blot analysis of mouse CNGA3 expression. Membrane preparations from cells transfected with mouse CNGA3 were resolved by 10% SDS−PAGE followed by Western blot analysis using the polyclonal anti-CNGA3 antibody. Loading control (actin) was included. (B) Expression of GFP-CNGA3 in HEK 293 cells detected by direct fluorescence microscopy (left panel) and immunostaining using the anti-CNGA3 antibody (right panel). Scale bar = 50 μm. (C) Intracellular calcium response to cGMP stimulation in HEK 293 cells transfected with CNGA3 cDNA. Cells (2×10^6) loaded with Indo-1/AM were stimulated with 8-pCPT-cGMP at various concentrations, and the signals were recorded using a PTI QuantaMaster spectrofluorometer (Photon Technology International).

CNGA3 antibody (1:50) in PBS with 5% BSA was added to the cells and incubated overnight at 4 °C. The primary antibody was washed for 3 × 10 min with PBS. Alexa-conjugated goat anti-rat secondary antibody (1:1000) in PBS with 1% BSA was then added to the cells for 1 h at room temperature and then washed for 3 × 10 min with PBS. Vectashield containing DAPI stain (Vector Laboratories) was used to mount the coverslips onto the slides.

The fluorescent signals were visualized using a 40× water immersion objective lens on an Olympus IX81-FV500 confocal laser scanning microscope (Olympus, Melville, NY) and analyzed with FluoView imaging software (Olympus). Quantification of cellular fluorescent labeling intensity was performed using FluoView to evaluate the cytosolic aggregation of CNGA3 in cells that have been treated with SPI-1. Multiple slices were taken at a thickness of 0.2 μm of cells. Using the intensity mapping feature of the software, cell slices with the highest localized fluorescent intensities in the intracellular area were chosen for further quantification. This measurement was achieved using the drawing tool to select the intracellular area(s) of high intensity, following calculation of the intensity by the software. The intensity of the entire area of the cell (meaning both intracellular area and plasma membrane) in that particular slice was then measured. From these intensity values, the level of cytosolic CNGA3 aggregation was determined and expressed in terms of percent of total cellular fluorescence intensity. Data were analyzed and graphed using GraphPad Prism software (GraphPad Software, San Diego, CA).

RESULTS

CNGA3 Expression, Plasma Membrane Localization, and Functional Activity in HEK 293 Cells. Mouse CNGA3 was heterologously established in HEK 293 cells, and expression, plasma membrane localization, and functional activity of the channel were examined by immunoblotting, immunolabeling, and ratiometric measurements of $[Ca^{2+}]_i$ in response to 8-pCPT-cGMP stimulation, respectively. Figure 1A shows Western blot analysis of expression of CNGA3 protein in transfected HEK 293 cells. The channel subunit migrated at a position of ~72 kDa as detected by the polyclonal anti-CNGA3 antibody. The proper plasma membrane localization of CNGA3 was confirmed by immunolabeling using the anti-CNGA3 antibody and by direct fluorescent microscopic examination of cells expressing GFP-CNGA3 (Figure 1B). Functional activity of CNGA3 in HEK 293 cells was demonstrated by ratiometric measurements of $[Ca^{2+}]_i$ in response to cGMP stimulation. Figure 1C shows representative traces of Indo-1/AM fluorescence measurements of $[Ca^{2+}]_i$ (shown as Δ340/380 fluorescence ratio) in response to increasing concentrations of 8-pCPT-cGMP in a population (2×10^6) of HEK 293 cells transfected with CNGA3 cDNA. No calcium mobilization was measured in a Ca^{2+}-free medium (see Supporting Information Figure 1).

Localization of CNGA3 to Low Buoyant Density, DRMs in HEK 293 Cells. To determine the detergent solubility of CNGA3, we solubilized membranes from CNGA3-expressing HEK 293 cells with Triton X-100 and OG. Figure 2A shows a significant amount of CNGA3 present in the detergent-insoluble pellet, following the detergent extraction (the detergent:membrane protein ratios for Triton X-100 and OG extraction were 3.3:1 and 5:1, respectively). Membranes solubilized with Triton X-100 at detergent:membrane protein ratios of 2.5:1 and 5.0:1 showed similar solubilization efficiency.

It is possible that the observed channel present in the pellet is due to interactions with cytoskeletal proteins. To investigate the possibility of a cytoskeletal interaction, membrane preparations were treated with potassium iodide (KI, 0.6 M), which is known to disrupt possible ionic interactions with the cytoskeleton (*34*). As shown in Figure 2B, pretreatment with KI did not increase the solubility of CNGA3 to Triton X-100, suggesting that the observed insolubility is not likely due to cytoskeletal association.

Proteins interacting with membrane microdomains have been shown to fractionate with low buoyant density membrane fractions following ice-cold Triton X-100 extraction while solubilized proteins and those linked to the cytoskeleton are recovered in higher density fractions (*18*). To determine whether insoluble CNGA3 is localized to such membranes, we isolated DRMs by sucrose density gradient ultracentrifugation as described in Experimental Procedures.

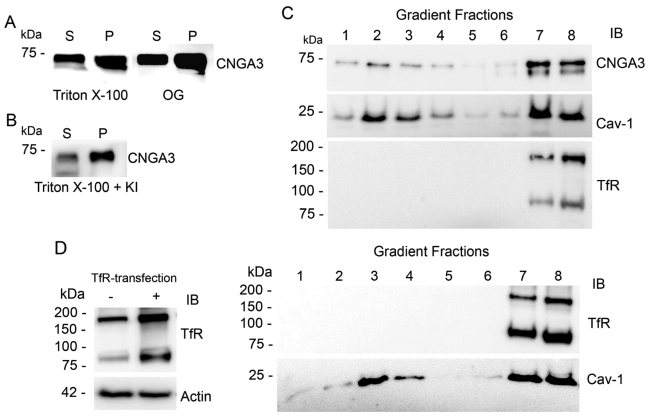

FIGURE 2: Localization of CNGA3 in low buoyant density, DRMs in HEK 293 cells. (A) Association of CNGA3 with detergent-resistant fractions of HEK 293 cell membranes. Membrane preparations from HEK 293 cells transfected with CNGA3 were solubilized by 1% Triton X-100 or 60 mM OG, and resultant supernatants (S) and pellets (P) were resolved by 10% SDS−PAGE, followed by Western blot analysis using the anti-CNGA3 antibody. (B) Effects of KI treatment on solubilization of CNGA3 by Triton X-100. Membrane preparations from transfected cells were solubilized by 1% Triton X-100 in the presence or absence of 0.6 M KI, and solubilized proteins were subjected to Western blot analysis. (C) Localization of CNGA3 in low buoyant density, DRMs in HEK 293 cells. The Triton X-100-solubilized cell lysates were fractionated on sucrose gradients, and the resulting fractions were analyzed by Western blot analysis using antibodies against CNGA3 (upper panel), caveolin-1 (Cav-1) (middle panel), and TfR (lower panel). (D) Absence of TfR in low buoyant density, DRMs prepared from HEK 293 cells that have been transfected with TfR cDNA. The left panel shows expression levels of TfR in cells with or without transfection of TfR cDNA. The right panel shows the gradient fractions analyzed by Western blotting using antibodies against TfR (upper panel) and Cav-1 (lower panel).

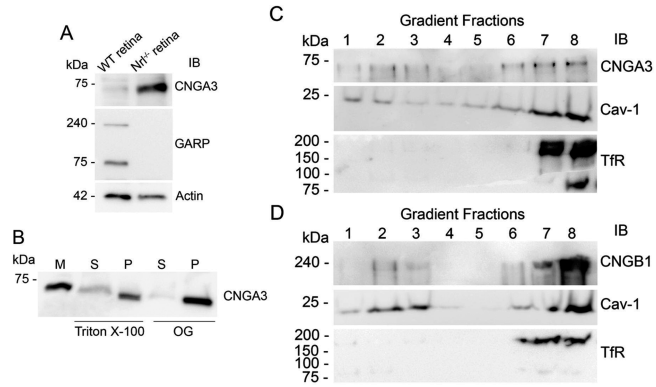

FIGURE 3: Localization of CNGA3 and CNGB1 in low buoyant density, DRMs in the mouse retina. (A) Expression of CNGA3 and CNGB1 in the mouse retina. Retinal membrane preparations from wild-type and $Nrl^{-/-}$ mice were resolved by 10% SDS−PAGE, followed by immunoblotting using the polyclonal anti-CNGA3 antibody (upper panel) and the monoclonal anti-GARP antibody (middle panel). Anti-GARP antibody detected CNGB1 (240 kDa band) and GARP2 (75 kDa band) in the wild-type but not $Nrl^{-/-}$ retina. Actin detection was performed as a loading control. (B) Association of CNGA3 with detergent-resistant fractions of $Nrl^{-/-}$ retina. Membrane preparations (M) from $Nrl^{-/-}$ retinas were solubilized by 1% Triton X-100 or 60 mM OG, and resultant supernatants (S) and pellets (P) were resolved by 10% SDS−PAGE, followed by Western blot analysis using the polyclonal anti-CNGA3 antibody. (C, D) Localization of CNGA3 (C) and CNGB1 (D) in low buoyant density, detergent-resistant membranes prepared from $Nrl^{-/-}$ and wild-type retinas, respectively. The Triton X-100-solubilized retinal membranes were fractionated on sucrose gradients, and the resulting fractions were analyzed by Western blot analysis using antibodies against CNGA3, GARP, caveolin-1, and TfR, respectively.

Immunoblotting of gradient fractions revealed two peaks of CNGA3 immunoreactivity (Figure 2C, upper panel). A significant portion of CNGA3 was found in the low buoyant density, detergent-resistant fractions (fractions 1–4) and was also present in the high-density, detergent-soluble fractions (fractions 7 and 8). This is consistent with the data in Figure 2A showing the presence of CNGA3 in both supernatant and pellets following detergent solubilization, and it may indicate that the cone channel is present in both detergent-soluble and detergent-resistant membrane domains. Of note, there is a second heavier band of CNGA3 in the higher density fractions (Figure 2C) [as well as in the detergent-soluble fraction (see Figure 2A,B)]. It was seen only in the heterologous expression system but not in retinas (see Figure 3). This band may be related to the glycosylation status of the CNGA3 subunit in a heterologous expression system. Under such experimental conditions, CNGA3 cofractionated with the lipid raft marker protein caveolin-1 in the low buoyant density fractions (peak at fraction 2) and in fractions 7–8 as well (Figure 2C, middle panel). The observation that a considerable amount of caveolin-1 was present in the high-density fractions may be related to the relatively high stringency of our detergent solubilization conditions used for DRM isolation. The detergent:lipid molar ratio used to isolate DRMs was 6:1 for HEK 293 cells (5:1 for retinas) when 1% Triton X-100 was used; this perhaps resulted in the solubilization of some DRM components which may contribute to the observed heavy proportion of caveolin-1 in fractions 7 and 8. This assumption is in agreement to the findings of Babiychuk and Draeger, who showed that increasing the concentration of Triton X-100 results in partial solubilization of caveolin-1 (*35*). To assess the purity of the DRMs isolated and ensure that they are not contaminated with non-DRM proteins, we examined the distribution of a known non-DRM-associated protein transferrin receptor (TfR) at both endogenous and overexpressed (from transfection) levels. The left panel of Figure 2D shows Western blot detection of TfR (monomer and dimer) in HEK 293 cells with or without transfection of TfR cDNA. These experiments showed that both endogenously expressed (Figure 2C) and overexpressed (Figure 2D, right panel) TfRs were absent from DRM fractions and were only detectable in high-density fractions.

Localization of CNGA3 and CNGB1 to Low Buoyant Density, DRMs in Mouse Retinas. To determine that the association of CNG channels to DRMs is not a function of expression in cell culture, we examined the fractionation of native CNG channels to DRMs isolated from the mouse retina. Retinas of $Nrl^{-/-}$ mice (cone-dominant) and wild-type mice (rod-dominant) were used to study the fractionation of cone and rod CNG channels, respectively. The polyclonal anti-CNGA3 antibody was used to detect CNGA3, and the monoclonal anti-GARP antibody was used to detect the modulatory subunit of the rod CNG channel (CNGB1). GARPs exist as two soluble forms, GARP1 and GARP2, and as an N-terminal large cytoplasmic domain (GARP-part) of CNGB1 and are known to be present in rods but not in cones. GARP2 is the most abundant splice form and is associated strongly with the membrane signaling proteins involved in phototransduction (such as phosphodiesterase and

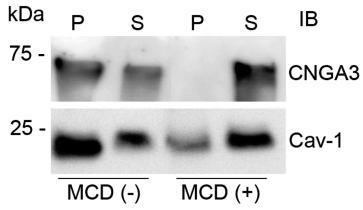

FIGURE 4: Effects of cholesterol depletion on solubility of CNGA3. HEK 293 cells transfected with CNGA3 cDNA were treated with 2% MCD at 37 °C for 1 h before they were harvested for Triton X-100 solubilization. The resultant supernatants (S) and pellets (P) were resolved by 10% SDS−PAGE, followed by immunoblotting using the respective antibodies.

guanylate cyclase) (*36*). Figure 3A shows Western blotting detected by anti-CNGA3 and anti-GARP antibodies. A single band of CNGA3 corresponding to an M_r of ~73 kDa (equivalent to the predicted size of 72.2 kDa) was detected in both $Nrl^{-/-}$ retina and wild-type retina, with the signal being more abundant in $Nrl^{-/-}$ retina than that in the wild type (Figure 3A, upper panel). This is consistent with the rod-dominant feature of wild-type mouse retina (cones comprise only 3–5% of the total photoreceptor population in wild-type mouse retina). Expression of CNGB1 (240 kDa band) and GARP2 (75 kDa band) was detected by the anti-GARP antibody in the wild-type but not $Nrl^{-/-}$ retina (Figure 3A, middle panel). Solubility of CNGA3 to Triton X-100 and OG extraction in $Nrl^{-/-}$ retinas was also examined. Membranes of $Nrl^{-/-}$ retinas were isolated and subjected to 1% Triton X-100 or 60 mM OG solubilization as described in Experimental Procedures. As observed in cultured cells, CNGA3 was poorly solubilized from the retinal membrane (Figure 3B), suggesting an association with DRMs.

Retinal membrane preparations from $Nrl^{-/-}$ (Figure 3C) and wild-type (Figure 3D) mice were then subjected to Triton X-100 solubilization, followed by sucrose gradient fractionation to prepare DRMs. As shown in Figure 3C,D, CNGA3 and CNGB1 cofractionated with caveolin-1 in both low (fractions 1–3) and high (fractions 7 and 8) density fractions. Similar to the results from HEK 293 cells, TfR was not detected in the DRMs fractionated from the mouse retinas (Figure 3C,D). Thus, the results using native channel preparations are consistent with the findings from the heterologous expression system, indicating that a pool of photoreceptor CNG channels is associated with detergent-resistant, caveolin-enriched membranes. This is in agreement with our recent proteomic analysis indicating the presence of CNGB1 and CNGA1 in DRMs isolated from bovine rod OS (*27*).

Effect of Cellular Cholesterol Depletion on the Solubility and Activity of CNGA3. It is known that cholesterol is enriched in lipid rafts and is required for their formation and structural integrity. To investigate the functional role of raft lipids on channel activity, we examined the effects of cholesterol depletion on the solubility and activity of CNGA3. Cholesterol depletion was achieved by incubating CNGA3-expressing HEK 293 with 2% MCD at 37 °C for 1 h before solubilization with 1% Triton X-100 and Western blot analysis. As shown in Figure 4, treatment with MCD increased the detergent solubilities of both CNGA3 (upper panel) and caveolin-1 (lower panel), suggesting that the membrane domains where these proteins reside were disrupted. It is worthy noting that the complete disappearance of CNGA3 from the pellet fraction and the presence of caveolin-1 in the pellet fraction after MCD treatment may suggest that the two proteins could reside in different types of membrane domains having different sensitivities to cholesterol depletion.

We then examined the effects of cholesterol depletion on channel activity. CNGA3-expressing HEK 293 cells were incubated with MCD as described and then harvested for intracellular calcium assays. As shown in the left panel of Figure 5A, MCD treatment significantly decreased the intracellular calcium response of these cells to cGMP stimulation. Similar results were also observed in cells expressing the rod CNGA1 subunit (Figure 5A, middle panel). The right panel shows quantitative analyses of calcium measurements at 500 s (CNGA3) and 400 s (CNGA1) after cGMP stimulation for the experiments shown in the left and middle panels, respectively.

To examine whether there is a difference in lipid raft association between homo- and heterochannel complexes, we examined the effects of MCD treatment on channel activity in cells cotransfected with CNGA3 and CNGB3 (the modulatory subunit of cone CNG channel) cDNAs. As shown in Figure 5B, treatment with MCD reduced the calcium response in the cotransfected cells as well, suggesting that both homo- and heterochannel complexes are modulated by raft lipids in this heterologous expression system. The right panel is a quantitative analysis of calcium measurements at 500 s after cGMP stimulation for the experiments shown in the left panel. Effects of MCD treatment were also examined in HeLa cells transfected with the mouse CNGA3 cDNA, and calcium responses were dramatically affected as well (see Supporting Information Figure 2), indicating that this modulation of channel activity was independent of the cell type chosen for heterologous expression. To further evaluate the specificity of the MCD treatment, cholesterol replacement experiments were performed. This was achieved by incubating CNGA3-bearing cells with 2% MCD in the presence of 0.5 mM cholesterol prior to calcium measurement. Figure 5C shows that cholesterol replacement almost completely reversed the effect of MCD treatment on the CNGA3 activation. The right panel is a quantitative analysis of calcium measurements at 400 s after cGMP stimulation for the experiments shown in the left panel.

Cellular cholesterol content and fatty acid profiles after MCD treatment were examined to demonstrate the effectiveness of cholesterol depletion and to determine whether the observed channel malfunction following MCD treatment is due to an overall alteration of membrane lipids. As shown in Figure 6, cellular cholesterol level was reduced by ~45% in cells following MCD treatment (Figure 6A) without altering the fatty acid profile (Figure 6B). Thus, MCD treatment does not result in gross changes in membrane lipid composition. These results indicate that the effect of MCD on channel activity most likely results from depletion of cholesterol in localized, cholesterol-enriched membrane microdomains.

Effects of Inhibition of Sphingolipid Biosynthesis on CNG Channel Activity and Plasma Membrane Localization. The effect of cholesterol depletion on channel function and the association of channel subunits with DRMs suggest that localization to membrane domains may be important in modulating channel activity. To further strengthen this

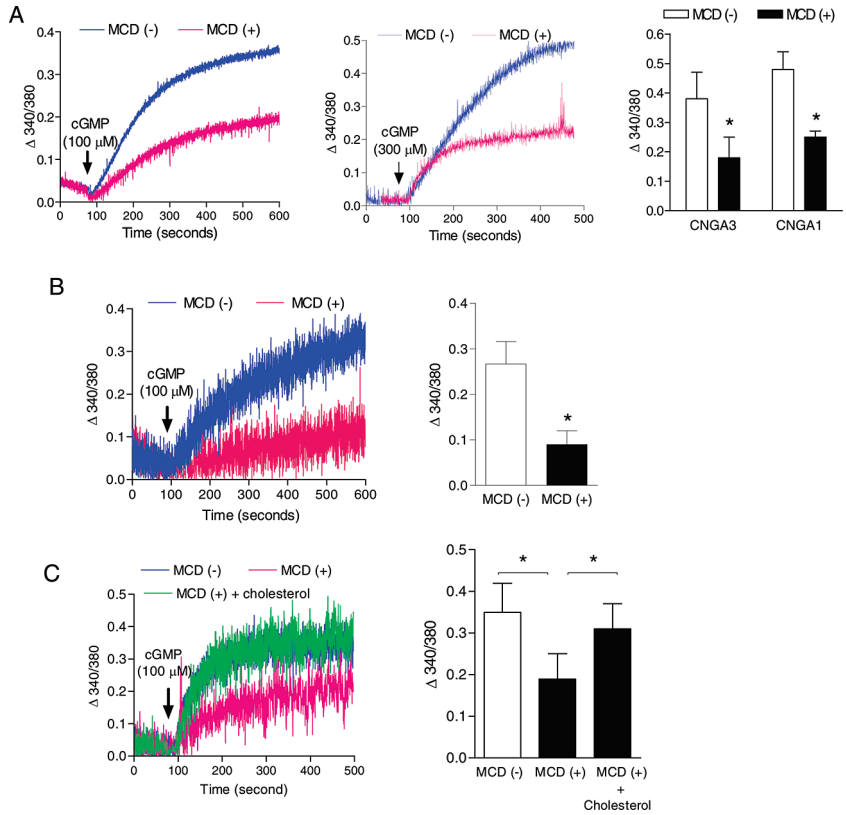

FIGURE 5: Effects of cholesterol depletion on the activity of the photoreceptor CNG channel. (A) MCD treatment impairs activation of the photoreceptor CNG channel evoked by cGMP stimulation. HEK 293 cells transfected with CNGA3 (left panel) and CNGA1 (middle panel) cDNAs, respectively, were treated with 2% MCD at 37 °C for 1 h and then subjected to ratiometric measurement of $[Ca^{2+}]_i$ in response to 8-pCPT-cGMP stimulation. The bar graph shows the quantitative analysis of the calcium measurement at 500 s (CNGA3) and 400 s (CNGA1) after 8-pCPT-cGMP stimulation in the experiments shown in the left and middle panels. (B) Effects of MCD treatment on the cGMP-evoked calcium response of HEK 293 cells transfected with CNGA3 and CNGB3 cDNAs. The right panel is a bar graph showing the quantitative analysis at 500 s after 8-pCPT-cGMP stimulation in the experiments shown in the left panel. (C) Cholesterol replacement reversed the effect of MCD treatment. Cells transfected with CNGA3 cDNA were treated with 2% MCD in the presence and absence of cholesterol (0.5 mM; Sigma) at 37 °C for 1 h followed by calcium assays. The bar graph shows the quantitative analysis at 400 s after 8-pCPT-cGMP stimulation in the experiments shown in the left panel. Bars represent the means ± SEM of assays of eight (CNGA3) and three (CNGA1) independently performed experiments in (A), three in (B), and four in (C). Unpaired Student's *t* test was used for determination of the significance. *, $p < 0.05$.

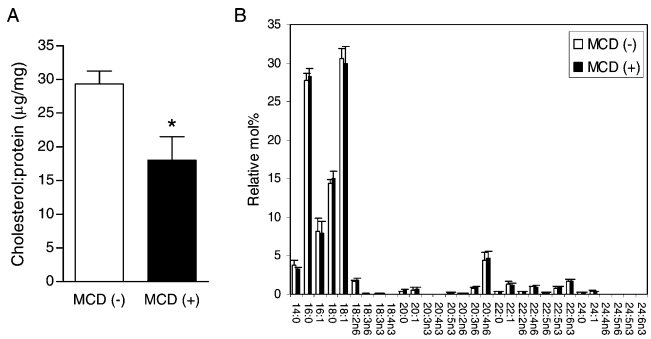

FIGURE 6: Effects of MCD treatment on levels of membrane cholesterol and fatty acids. HEK 293 cells were treated with 2% MCD at 37 °C for 1 h and then harvested for analysis of membrane cholesterol (A) and fatty acid (B) levels, using a two-part extraction procedure to separate saponifiable from nonsaponifiable lipids. Bars represent the means ± SEM of assays of seven independently preformed experiments. Unpaired Student's *t* test was used for determination of the significance. *, $p < 0.05$.

hypothesis, we examined the effect of a second class of raft lipids, sphingolipids, on CNGA3 function and plasma membrane localization. Myriocin (SPI-1) is a metabolic inhibitor for the synthesis of ceramide, which is a common precursor of all complex sphingolipids, including glycosphingolipids (GSLs) and sphingomyelin (SM) (both known to be present in membrane microdomains). Treatment with SPI-1 can exclude the possibility that metabolic intermediates affect the protein function as it blocks the initial step of sphingolipid biosynthesis. As shown in Figure 7A, treatment of CNGA3-expressing cells with SPI-1 significantly inhibited calcium influx in response to 8-pCPT-cGM stimulation. The response to 100 μM 8-pCPT-cGMP stimulation was significantly decreased while the response to 30 μM 8-pCPT-cGMP was almost completely abolished (Figure 7A, left panel). The right panel shows quantitative analysis of the calcium measurement at 400 s after stimulation with 100 μM 8-pCPT-cGMP. To explore whether the observed reduction in the calcium influx rate is attributed to a reduced number of active channels in the plasma membrane, we incubated CNGA3-bearing cells (that had been pretreated with SPI-1 for 72 h) with a supersaturating level (1.0 mM) of 8-pCPT-cGMP in the absence of Ca^{2+} and then measured the calcium influx upon readdition of Ca^{2+} (200 μM). Figure 7B shows that, under these experimental conditions, the calcium influx rate was significantly lowered (~40% reduction) in cells that had been treated with SPI-1 compared to the untreated cells (left and middle panels). A small calcium influx was observed in the untransfected cells that had been incubated in 8-pCPT-cGMP under the same conditions, both with and without

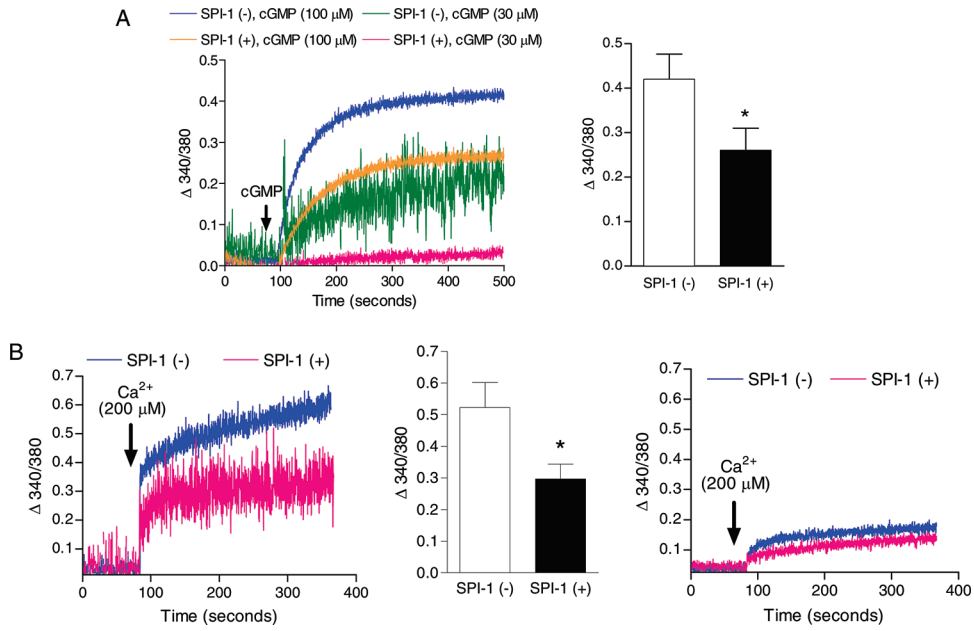

FIGURE 7: Effects of inhibition of sphingolipid biosynthesis on CNGA3 activity. Cells were treated with the sphingolipid biosynthesis inhibitor SPI-1 (5 μM) for 72 h before they were harvested for calcium assay. (A) Treatment with SPI-1 inhibited calcium response to 8-pCPT-cGMP stimulation. The bar graph shows the quantitative analysis of the calcium measurement at 400 s after 8-pCPT-cGMP (100 μM) stimulation in the experiments shown in the left panel. (B) Treatment with SPI-1 (5 μM, 72 h) inhibited the calcium influx in cells that have been preincubated in supersaturating (1.0 mM) 8-pCPT-cGMP for 1 h in the absence of Ca^{2+}, followed by the addition of 200 μM Ca^{2+} (left panel). The bar graph shows the quantitative analysis of the calcium measurement at 300 s after addition of Ca^{2+} in the experiments shown in the left panel. A small calcium influx was observed in transfected cells that have been incubated in 8-pCPT-cGMP (1 mM) after addition of 200 μM Ca^{2+}, both with and without SPI-1 pretreatment (right panel). Bars represent the means ± SEM of assays of three independently performed experiments. Unpaired Student's *t* test was used for determination of the significance. *, $p < 0.05$.

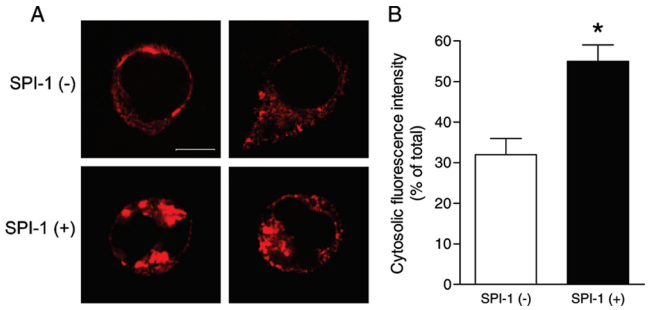

FIGURE 8: Effects of inhibition of sphingolipid biosynthesis on membrane localization in HEK 293 cells. Cells were treated with the sphingolipid biosynthesis inhibitor SPI-1 (5 μM) for 72 h before the immunofluorescence labeling. The images were taken by confocal microscopy and analyzed using the FluoView imaging software. (A) Representative images of immunofluorescence labeling of CNGA3 in HEK 293 cells that have been treated with SPI-1. Scale bar = 10 μm. (B) The bar graph shows the quantitative analysis results of the cellular fluorescence labeling intensity. Bars represent the means ± SEM of the number of cells (19 for SPI-1-treated cells and 13 for the untreated cells) from three independently performed experiments. Unpaired Student's *t* test was used for determination of the significance. *, $p < 0.05$.

SPI-1 pretreatment (right panel). These results support the hypothesis that perturbation of the membrane domains by SPI-1 treatment likely results in reduced numbers of active channels in the plasma membrane.

We next examined the effects of SPI-1 treatment on the CNGA3 plasma membrane localization. The cellular distribution of CNGA3 was examined in cells treated with and without SPI-1 (5 μM) for 72 h by immunofluoresecence labeling and confocal microscopy. As shown in Figure 8, mislocalization and cellular aggregation of CNGA3 was observed in cells that had been treated with SPI-1. Quantitative analysis of the confocal images indicates that the fluorescence intensity of the cytosolic aggregates (expressed as percent of total cellular fluorescence intensity) in cells treated with SPI-1 is 55%, which is significantly higher than that in the untreated cells (31%) (Figure 8, right panel). Thus, it appears that inhibition of sphingolipid biosynthesis leads to impaired cellular processing and plasma membrane localization of CNGA3, which may contribute to the observed perturbation of channel function.

DISCUSSION

Membrane microdomains rich in tightly packed sphingolipids and cholesterol are present in both excitable and nonexcitable cells and in species ranging from yeast to humans (*19, 37*). A variety of membrane signaling molecules including G protein-coupled receptors (*21, 38*), ion channels (*17*), and protein kinases (*20*) are found in these specialized membranes. This work shows localization of photoreceptor CNG channels to DRMs. Due to the following observations this is less likely a function of overexpression but rather has biological significance. (1) CNGA3 was targeted to DRMs equally well in HEK 293 cells, when expressed at both low and high levels, as determined by transfection of different amounts of cDNA into the cells (20 μg of cDNA per 100 mm dish vs 10 μg of cDNA per 100 mm dish) (see Supporting Information Figure 3 for results from 10 μg of cDNA transfection). (2) TfR at both the endogenously expressed level (in HEK 293 cells as well as in retinas) and overexpressed level was absent in the DRMs but present in the high-density fractions. (3) Localization of the CNG channel in the DRMs was also observed in the mouse retinal preparations. (4) Our later results demonstrated a functional significance to levels of the two DRM-enriched lipid species,

cholesterol and sphingolipids, showing preferential partitioning to DRMs. The observation of inhibition of photoreceptor CNG channel function by depletion of cellular cholesterol is consistent with studies on the analogous olfactory CNG channel described by Brady et al. (*15*) In this study the A subunit of the olfactory CNG channel (CNGA2) was found to associate with DRMs in heterologous expression systems and in rat olfactory epithelium, and cholesterol depletion abolished prostaglandin-stimulated CNGA2 channel activity in intact cells. In the present study, the role of raft lipids on photoreceptor CNG channel modulation was further demonstrated by inhibition of sphingolipid biosynthesis. Such treatment resulted in an inhibition of channel function and cytosolic aggregation of the channel. Thus, this work demonstrates for the first time a modulatory role of cholesterol- and sphingolipid-enriched membrane domains on photoreceptor CNG channel function.

Lipid rafts are proposed to serve as scaffolding regions where signal transduction pathways interface (*20*), and association of signaling proteins with membrane domains may facilitate their coassembly into signaling complexes. In addition, microdomains might have unique biophysical properties that directly affect the functions of signaling proteins. Some of these parameters include lateral pressure profile, bilayer fluidity, bilayer thickness, and surface charge (*39*). Specifically the involvement of lipid rafts in cell surface compartmentation appears to be a mechanism for the polarized sorting of some neuronal proteins (*19*). Cholesterol depletion or deprivation of membrane sphingolipids almost certainly disrupts interactions between the membrane signaling molecules and the lipid bilayer, either in the form of specific protein–lipid interactions or through changes in the physical properties of the bilayer itself (*40*). Such alterations might bring about mislocalization of the protein or directly affect allosteric conformational changes involved in activation (or channel opening) and/or affinity of the ligand binding, which in turn lead to protein malfunction. Blasquez et al. (*41*) previously found that depletion of sphingolipids resulted in missorting of prohormone convertase 2 (a protease of the regulated secretory pathway involved in the intracellular maturation of prohormones). Impaired membrane localization of CNGA3 following deprivation of sphingolipids was shown in this study while a negative effect of cholesterol depletion on cAMP binding affinity was described previously for the olfactory CNGA2 channel (*15*). Blockade of Trp1 channel opening (*42*) and impaired inactivation but not activation of the shaker-like potassium channel (*23*) following depletion of cellular cholesterol have been previously described as well. Thus, mechanisms behind the functional dependence of ion channel activity on constituent membrane lipids may vary for different channels. The present study shows a mislocalization of CNGA3 following inhibition of sphingolipid biosynthesis, suggesting that cell surface compartmentation and membrane targeting may represent a role of lipid rafts in photoreceptor CNG channel function and signaling.

Association of membrane proteins with lipid rafts may involve different mechanisms. It has been suggested that membrane proteins are targeted to lipid raft domains either by interaction with raft proteins (such as caveolin-1 and PSD-95) (*17, 42, 43*) or with raft lipids (*39, 44, 45*). Posttranslational modifications (including acylation, palmitoylation, and myristoylation) of peripheral membrane proteins or glycophosphatidylinositol (GPI) membrane anchors are thought to be involved in such associations (*46*). This has been observed mainly for monotopic proteins, and much less is known about the molecular mechanisms that target polytopic proteins to lipid rafts. Questions about how photoreceptor CNG channels are targeted to or associate with lipid rafts and whether posttranslational modification of channel subunits are involved remain to be addressed. Although immunoprecipitation experiments in this study did not show evidence of direct interaction between CNGA3 and caveolin-1 (data not shown), the role of caveolin-1 in the association of the channel with the membrane microdomain cannot be excluded. It is also possible that such association is via other raft-associating proteins or with raft lipids.

Impaired membrane localization of cell surface functional proteins represents a common mechanism of protein dysfunction, and this phenomenon has been observed in a variety of disease-causing mutations (*10, 11, 47, 48*). There are a number of mechanisms involved in peripheral protein membrane surface sorting and targeting, and association with lipid rafts might be one of them. Mutations in CNG channels may interfere with their interactions with membrane microdomains which may, in turn, interfere with protein membrane surface sorting. A number of mutations have been found to result in mislocalization of the rod and cone photoreceptor CNG channel (*10, 11*). It is important to examine whether these residues are involved in membrane microdomain association.

Although the present study supports the importance of the integrity of cholesterol- and sphingolipid-rich membranes in photoreceptor CNG channel activity, it appears that not all CNG channels are localized to DRMs. A considerable amount of the channel was identified in the high-density, soluble fractions of a sucrose gradient, suggesting the existence of the channel protein in both DRMs and non-DRMs. Whether the channels are homogeneously distributed in these different domains or enriched in DRMs remains to be addressed. The biochemical isolation of DRMs is a qualitative, not a quantitative, assessment of protein affinity for caveolin-1- and cholesterol-rich, detergent-insoluble membranes (*49*). For this reason, it is difficult to calculate the fraction of CNGA3 channels that resides in DRMs and non-DRMs based on our biochemical data. However, the functional association of the integrity of the cholesterol- and sphingolipid-enriched membrane domains with the channel's activity suggests that localization of the photoreceptor CNG channel to the DRMs is less likely a random event but has biological significance. It seems that a proportion of the channel has preference for an ordered, cholesterol-rich environment. Whether the channels that reside in DRMs and non-DRMs are all functional is not known, and the dynamic relationship of the channel between the two different membrane microdomains remains to be addressed.

This study demonstrates that cone and rod photoreceptor CNG channels are associated with DRMs and that depletion of DRM-rich lipids dramatically impairs the channel's activity. Cytosolic aggregation of the channel was observed when cells were treated with the sphingolipid biosynthesis inhibitor, implicating a role of raft lipids in the channel cellular processing. These findings establish the importance of the local lipid environment on photoreceptor CNG channel

cellular processing and function. It remains to be determined whether disease-causing mutations affect the localization of cone and rod CNG channels to the membrane microdomains.

ACKNOWLEDGMENT

We thank Drs. Anand Swaroop, Martin Biel, William Zagotta, Michael Marks, Benjamin Kaupp, and Robert Molday for providing $Nrl^{-/-}$ mice, mouse CNGB3 cDNA, human CNGA1 cDNA, human TfR cDNA, the rat monoclonal anti-CNGA3 antibody, and the monoclonal anti-GARP antibody, respectively. We thank Mr. Alexander Quiambao for providing excellent technical assistance. We also thank Drs. Leonidas Tsiokas and Muayyad Al-Ubaidi for support in facilitating the experiments.

SUPPORTING INFORMATION AVAILABLE

Three figures as described in the text. This material is available free of charge via the Internet at http://pubs.acs.org.

REFERENCES

1. Yau, K. W., and Baylor, D. A. (1989) Cyclic GMP-activated conductance of retinal photoreceptor cells. *Annu. Rev. Neurosci. 12*, 289–327.
2. Cook, N. J., Molday, L. L., Reid, D., Kaupp, U. B., and Molday, R. S. (1989) The cGMP-gated channel of bovine rod photoreceptors is localized exclusively in the plasma membrane. *J. Biol. Chem. 264*, 6996–6999.
3. Kaupp, U. B., Niidome, T., Tanabe, T., Terada, S., Bonigk, W., Stuhmer, W., Cook, N. J., Kangawa, K., Matsuo, H., Hirose, T., et al. (1989) Primary structure and functional expression from complementary DNA of the rod photoreceptor cyclic GMP-gated channel. *Nature 342*, 762–766.
4. Arshavsky, V. Y., Lamb, T. D., and Pugh, E. N., Jr. (2002) G proteins and phototransduction. *Annu. Rev. Physiol. 64*, 153–187.
5. Bareil, C., Hamel, C. P., Delague, V., Arnaud, B., Demaille, J., and Claustres, M. (2001) Segregation of a mutation in CNGB1 encoding the beta-subunit of the rod cGMP-gated channel in a family with autosomal recessive retinitis pigmentosa. *Hum. Genet. 108*, 328–334.
6. Dryja, T. P., Finn, J. T., Peng, Y. W., McGee, T. L., Berson, E. L., and Yau, K. W. (1995) Mutations in the gene encoding the alpha subunit of the rod cGMP-gated channel in autosomal recessive retinitis pigmentosa. *Proc. Natl. Acad. Sci. U.S.A. 92*, 10177–10181.
7. Nishiguchi, K. M., Sandberg, M. A., Gorji, N., Berson, E. L., and Dryja, T. P. (2005) Cone cGMP-gated channel mutations and clinical findings in patients with achromatopsia, macular degeneration, and other hereditary cone diseases. *Hum. Mutat. 25*, 248–258.
8. Wissinger, B., Gamer, D., Jagle, H., Giorda, R., Marx, T., Mayer, S., Tippmann, S., Broghammer, M., Jurklies, B., Rosenberg, T., Jacobson, S. G., Sener, E. C., Tatlipinar, S., Hoyng, C. B., Castellan, C., Bitoun, P., Andreasson, S., Rudolph, G., Kellner, U., Lorenz, B., Wolff, G., Verellen-Dumoulin, C., Schwartz, M., Cremers, F. P., Apfelstedt-Sylla, E., Zrenner, E., Salati, R., Sharpe, L. T., and Kohl, S. (2001) CNGA3 mutations in hereditary cone photoreceptor disorders. *Am. J. Hum. Genet. 69*, 722–737.
9. Kaupp, U. B., and Seifert, R. (2002) Cyclic nucleotide-gated ion channels. *Physiol. Rev. 82*, 769–824.
10. Faillace, M. P., Bernabeu, R. O., and Korenbrot, J. I. (2004) Cellular processing of cone photoreceptor cyclic GMP-gated ion channels: a role for the S4 structural motif. *J. Biol. Chem. 279*, 22643–22653.
11. Trudeau, M. C., and Zagotta, W. N. (2002) An intersubunit interaction regulates trafficking of rod cyclic nucleotide-gated channels and is disrupted in an inherited form of blindness. *Neuron 34*, 197–207.
12. Hasegawa, H., Yang, Z., Oltedal, L., Davanger, S., and Hay, J. C. (2004) Intramolecular protein-protein and protein-lipid interactions control the conformation and subcellular targeting of neuronal Ykt6. *J. Cell Sci. 117*, 4495–4508.
13. Wenk, M. R., and De Camilli, P. (2004) Protein-lipid interactions and phosphoinositide metabolism in membrane traffic: insights from vesicle recycling in nerve terminals. *Proc. Natl. Acad. Sci. U.S.A. 101*, 8262–8269.
14. Rajala, R. V., Chan, M. D., and Rajala, A. (2005) Lipid-protein interactions of growth factor receptor-bound protein 14 in insulin receptor signaling. *Biochemistry 44*, 15461–15471.
15. Brady, J. D., Rich, T. C., Le, X., Stafford, K., Fowler, C. J., Lynch, L., Karpen, J. W., Brown, R. L., and Martens, J. R. (2004) Functional role of lipid raft microdomains in cyclic nucleotide-gated channel activation. *Mol. Pharmacol. 65*, 503–511.
16. Bruses, J. L., Chauvet, N., and Rutishauser, U. (2001) Membrane lipid rafts are necessary for the maintenance of the (alpha)7 nicotinic acetylcholine receptor in somatic spines of ciliary neurons. *J. Neurosci. 21*, 504–512.
17. Martens, J. R., Sakamoto, N., Sullivan, S. A., Grobaski, T. D., and Tamkun, M. M. (2001) Isoform-specific localization of voltage-gated K^+ channels to distinct lipid raft populations. Targeting of Kv1.5 to caveolae. *J. Biol. Chem. 276*, 8409–8414.
18. Brown, D. A., and London, E. (2000) Structure and function of sphingolipid- and cholesterol-rich membrane rafts. *J. Biol. Chem. 275*, 17221–17224.
19. Ikonen, E. (2001) Roles of lipid rafts in membrane transport. *Curr. Opin. Cell Biol. 13*, 470–477.
20. Simons, K., and Ikonen, E. (1997) Functional rafts in cell membranes. *Nature 387*, 569–572.
21. Simons, K., and Toomre, D. (2000) Lipid rafts and signal transduction. *Nat. Rev. Mol. Cell. Biol. 1*, 31–39.
22. Yarbrough, T. L., Lu, T., Lee, H. C., and Shibata, E. F. (2002) Localization of cardiac sodium channels in caveolin-rich membrane domains: regulation of sodium current amplitude. *Circ. Res. 90*, 443–449.
23. Martens, J. R., Navarro-Polanco, R., Coppock, E. A., Nishiyama, A., Parshley, L., Grobaski, T. D., and Tamkun, M. M. (2000) Differential targeting of Shaker-like potassium channels to lipid rafts. *J. Biol. Chem. 275*, 7443–7446.
24. Rybin, V. O., Xu, X., Lisanti, M. P., and Steinberg, S. F. (2000) Differential targeting of beta-adrenergic receptor subtypes and adenylyl cyclase to cardiomyocyte caveolae. A mechanism to functionally regulate the cAMP signaling pathway. *J. Biol. Chem. 275*, 41447–41457.
25. Magee, T., Pirinen, N., Adler, J., Pagakis, S. N., and Parmryd, I. (2002) Lipid rafts: cell surface platforms for T cell signaling. *Biol. Res. 35*, 127–131.
26. Martens, J. R., O'Connell, K., and Tamkun, M. (2004) Targeting of ion channels to membrane microdomains: localization of KV channels to lipid rafts. *Trends Pharmacol. Sci. 25*, 16–21.
27. Elliott, M. H., Nash, Z. A., Takemori, N., Fliesler, S. J., McClellan, M. E., and Naash, M. I. (2008) Differential distribution of proteins and lipids in detergent-resistant and detergent-soluble domains in rod outer segment plasma membranes and disks. *J. Neurochem. 104*, 352.
28. Huttl, S., Michalakis, S., Seeliger, M., Luo, D. G., Acar, N., Geiger, H., Hudl, K., Mader, R., Haverkamp, S., Moser, M., Pfeifer, A., Gerstner, A., Yau, K. W., and Biel, M. (2005) Impaired channel targeting and retinal degeneration in mice lacking the cyclic nucleotide-gated channel subunit CNGB1. *J. Neurosci. 25*, 130–138.
29. Mears, A. J., Kondo, M., Swain, P. K., Takada, Y., Bush, R. A., Saunders, T. L., Sieving, P. A., and Swaroop, A. (2001) Nrl is required for rod photoreceptor development. *Nat. Genet. 29*, 447–452.
30. Martin, R. E., Elliott, M. H., Brush, R. S., and Anderson, R. E. (2005) Detailed characterization of the lipid composition of detergent-resistant membranes from photoreceptor rod outer segment membranes. *Invest. Ophthalmol. Visual Sci. 46*, 1147–1154.
31. Elliott, M. H., Fliesler, S. J., and Ghalayini, A. J. (2003) Cholesterol-dependent association of caveolin-1 with the transducin alpha subunit in bovine photoreceptor rod outer segments: disruption by cyclodextrin and guanosine 5′-*O*-(3-thiotriphosphate). *Biochemistry 42*, 7892–7903.
32. Ma, R., Li, W. P., Rundle, D., Kong, J., Akbarali, H. I., and Tsiokas, L. (2005) PKD2 functions as an epidermal growth factor-activated plasma membrane channel. *Mol. Cell. Biol. 25*, 8285–8298.
33. Stricker, H. M., Ding, X. Q., Quiambao, A., Fliesler, S. J., and Naash, M. I. (2005) The Cys214→Ser mutation in peripherin/rds causes a loss-of-function phenotype in transgenic mice. *Biochem. J. 388*, 605–613.
34. Campbell, K. P., and Kahl, S. D. (1989) Association of dystrophin and an integral membrane glycoprotein. *Nature 338*, 259–262.

35. Babiychuk, E. B., and Draeger, A. (2006) Biochemical characterization of detergent-resistant membranes: a systematic approach. *Biochem. J. 397*, 407–416.
36. Korschen, H. G., Beyermann, M., Muller, F., Heck, M., Vantler, M., Koch, K. W., Kellner, R., Wolfrum, U., Bode, C., Hofmann, K. P., and Kaupp, U. B. (1999) Interaction of glutamic-acid-rich proteins with the cGMP signalling pathway in rod photoreceptors. *Nature 400*, 761–766.
37. Bagnat, M., Keranen, S., Shevchenko, A., and Simons, K. (2000) Lipid rafts function in biosynthetic delivery of proteins to the cell surface in yeast. *Proc. Natl. Acad. Sci. U.S.A. 97*, 3254–3259.
38. Jacobson, K., and Dietrich, C. (1999) Looking at lipid rafts? *Trends Cell Biol. 9*, 87–91.
39. McIntosh, T. J., and Simon, S. A. (2006) Roles of bilayer material properties in function and distribution of membrane proteins. *Annu. Rev. Biophys. Biomol. Struct. 35*, 177–198.
40. Martinac, B., and Hamill, O. P. (2002) Gramicidin A channels switch between stretch activation and stretch inactivation depending on bilayer thickness. *Proc. Natl. Acad. Sci. U.S.A. 99*, 4308–4312.
41. Blazquez, M., Thiele, C., Huttner, W. B., Docherty, K., and Shennan, K. I. (2000) Involvement of the membrane lipid bilayer in sorting prohormone convertase 2 into the regulated secretory pathway. *Biochem. J. 349*, 843–852.
42. Lockwich, T. P., Liu, X., Singh, B. B., Jadlowiec, J., Weiland, S., and Ambudkar, I. S. (2000) Assembly of Trp1 in a signaling complex associated with caveolin-scaffolding lipid raft domains. *J. Biol. Chem. 275*, 11934–11942.
43. Wong, W., and Schlichter, L. C. (2004) Differential recruitment of Kv1.4 and Kv4.2 to lipid rafts by PSD-95. *J. Biol. Chem. 279*, 444–452.
44. Scheiffele, P., Roth, M. G., and Simons, K. (1997) Interaction of influenza virus haemagglutinin with sphingolipid-cholesterol membrane domains via its transmembrane domain. *EMBO J. 16*, 5501–5508.
45. Lundbaek, J. A., Andersen, O. S., Werge, T., and Nielsen, C. (2003) Cholesterol-induced protein sorting: an analysis of energetic feasibility. *Biophys. J. 84*, 2080–2089.
46. Melkonian, K. A., Ostermeyer, A. G., Chen, J. Z., Roth, M. G., and Brown, D. A. (1999) Role of lipid modifications in targeting proteins to detergent-resistant membrane rafts. Many raft proteins are acylated, while few are prenylated. *J. Biol. Chem. 274*, 3910–3917.
47. Taylor, J. P., Metcalfe, R. A., Watson, P. F., Weetman, A. P., and Trembath, R. C. (2002) Mutations of the PDS gene, encoding pendrin, are associated with protein mislocalization and loss of iodide efflux: implications for thyroid dysfunction in Pendred syndrome. *J. Clin. Endocrinol. Metab. 87*, 1778–1784.
48. Yan, F., Lin, C. W., Weisiger, E., Cartier, E. A., Taschenberger, G., and Shyng, S. L. (2004) Sulfonylureas correct trafficking defects of ATP-sensitive potassium channels caused by mutations in the sulfonylurea receptor. *J. Biol. Chem. 279*, 11096–11105.
49. Shogomori, H., and Brown, D. A. (2003) Use of detergents to study membrane rafts: the good, the bad, and the ugly. *Biol. Chem. 384*, 1259–1263.

BI7019645